Applied Catalysis B: Environmental 201 (2017) 41–47

Contents lists available at ScienceDirect

Applied Catalysis B: Environmental

journal homepage: www.elsevier.com/locate/apcatb

Aerosol spray assisted assembly of TiO_2 mesocrystals into hierarchical hollow microspheres with enhanced photocatalytic performance

Chao Tang [1], Longfei Liu [1], Yali Li, Zhenfeng Bian *

The Education Ministry Key Lab of Resource Chemistry and Shanghai Key Laboratory of Rare Earth Functional Materials, Shanghai Normal University, Shanghai, 200234, PR China

ARTICLE INFO

Article history:
Received 30 June 2016
Received in revised form 1 August 2016
Accepted 2 August 2016
Available online 8 August 2016

Keywords:
Aerosol spray
TiO_2 Mesocrystals
Photocatalysis
Au nanoparticles
Hollow structure

ABSTRACT

TiO_2 mesocrystals significantly enhanced the charge separation owing to the oriented superstructures (less internal defects) and porous properties (more active sites), which was useful for applications from photocatalysis to optoelectronics. In this work, ultrasound assisted aerosol-spray method followed by topotactic transformations was adopted to fabricate TiO_2 hierarchical hollow microspheres. The unique structure was assembled by TiO_2 mesocrystal nanosheets. The TiO_2 mesocrystal hollow microspheres can greatly improve the photocatalytic performance. Furthermore, with the addition of Au^{3+} species in the precursor solution, ultrafine Au nanoparticles (3–4 nm) were uniformly deposited on the surface of TiO_2 hollow microspheres. It shows great significance for the development and application of the TiO_2 mesocrystals.

1. Introduction

Photocatalysis is one method of the advanced oxidation processes (AOP), which is also a potential technology for solving environmental and energy problems including degradation of pollutants, water splitting and dye-sensitized solar cell [1–4]. It is well established that an efficient photocatalyst is the principal part for photocatalysis process. Among various semiconductor photocatalysts, TiO_2 is desirable for photocatalytic application owing to its peculiarities of stability, low cost, and nontoxicity [5–7]. TiO_2 mesocrystals have recently emerged and been paid more and more attention as a new class of porous TiO_2 materials with oriented superstructures arranged by TiO_2 nanocrystal building blocks [8–18]. Recently, our work showed that TiO_2 mesocrystals could largely enhance charge separation and had remarkably long-lived charges, thereby exhibiting greatly increased photoconductivity and photocatalytic activity [8–11].

Varied synthetic strategies have been emerged to successfully synthesize TiO_2 mesocrystals in the past few years [9,11–18]. It is important to note that TiO_2 mesocrystals were first synthesized by O'Brien's group using topotactic conversion from NH_4TiOF_3 mesocrystals [17]. Recently, hydrothermal/solvothermal approaches were most commonly used to synthesize TiO_2 mesocrystals [11–18]. Although it is beneficial to obtain high quality TiO_2 mesocrystals at a specific temperature and for a period, these methods included complicated procedures which lead to the limitation in their large-scale applications.

On the other hand, aerosol spray has received a lot of interest mainly because it is a rapid method for synthesis of nano-materials [19–27]. The atomizer creates an aerosol mist of liquid droplets including the precursor of nano-materials. In a certain temperature, the droplets evaporate rapidly, resulting in very fine particles of nano-materials. Until now, by varying the precursors, surfactant and solvent, SiO_2, TiO_2, carbon, $Bi_2Ti_2O_7$ and other nano-materials have been successfully fabricated with mesoporous structure [19–27]. Despite the excellent potentialities of aerosol spray for the preparation of nano-materials, there have been very few studies on the preparation of single crystal materials. Very recently, Ohtani et al. demonstrated that single-crystalline anatase particles with decahedral structure could be synthesized by a gas-phase reaction [28]. However, the gas-phase reaction described by Ohtani et al. can only obtain bulk TiO_2 single crystals with no porosity. Porous TiO_2 single crystals with a relatively large specific surface area is still highly desired through a facile and easy to handle method.

Here, we developed an ultrasound-assisted aerosol spray approach to synthesize hierarchical TiO_2 mesocrystals hollow microspheres. By controlling the spray drying temperatures, TiO_2 nanosheets mesocrystals were self-assembled into hierarchical hollow microspheres due to the template effect of the spray

* Corresponding author.
E-mail addresses: bianzhenfeng@shnu.edu.cn, bianzhenfeng@163.com (Z. Bian).
[1] Equal contribution as the first author.

http://dx.doi.org/10.1016/j.apcatb.2016.08.006
0926-3373/

droplets. The results revealed that the hollows microspheres had an average diameter in the range of 0.5–2 μm. The TiO_2 mesocrystal hollow microspheres were displayed enhanced photocatalytic activity in comparison with TiO_2 nanosheet mesocrystals. Furthermore, we found that it was a general method to incorporating guest metal nanoparticles such as Au in TiO_2 mesocrystal hollow structures when the metal precursor solution was involved. The surface modification of ultrafine Au nanoparticles greatly improved the visible light responsive photocatalytic activity.

2. Experimental

2.1. Materials

P123 ($(EO)_{20}(PO)_{70}(EO)_{20}$), TiF_4 were purchased from Aldrich. NH_4NO_3, NH_4F, $HAuCl_4$, methyl orange (MO) and *p*-chlorophenol (4-CP) (AR) were purchased from Sinopharm Chemical Reagent Co., Ltd. All the reagents were used as received without further purification.

2.2. Preparation of hierarchical TiO_2 mesocrystals

A precursor solution containing TiF_4, H_2O, NH_4NO_3, and P123 with molar ratio of 90:30000:450:1 was prepared. The precursor solution was ultrasonically atomized into aerosol droplets by a household ultrasonic humidifier (1.7 MHz, 50VA), followed by passing through a quartz glass tube in tubular furnace at 400 °C with the air carrier gas. The solid product was filtered and collected, followed by calcination at a desired temperature in the range of 200–900 °C for 2 h.

Nanosheet TiO_2 mesocrystals as a control sample was prepared by the same aerosol spray method with NH_4F (TiF_4:NH_4F = 1:10 (molar ratio)) in the precursor solution. The obtained precipitate was then calcined at 800 °C for 2 h.

2.3. Preparation of Au/TiO_2 mesocrystals

A certain amount of $HAuCl_4$ was added into the precursor solution of hierarchical TiO_2 mesocrystals to adjust the molar ratio of Au/TiO_2. After aerosol spray, the solid product was filtered and collected, followed by calcination at 500 °C for 2 h.

2.4. Characterizations

The samples were characterized using X-ray diffraction (XRD, Rigaku D/MAX-2000, CuKα source), scanning electron microscopy (SEM, HITACHI S4800), transmission electronic micrograph (TEM, JEOL JEM-2010, operated at 200 kV) and nitrogen sorption (Micromeritics Instrument Corporation, Tristar II 3020, at 77 K). The Brunauer-Emmett-Teller (BET) method was utilized to calculate the specific surface area. The pore volume and pore diameter distribution were derived from the desorption isotherms by the Barrett-Joyner-Halenda (BJH) model. X-ray photoelectron spectroscopy (XPS, Versa ProbePHI 5000) was employed to determine surface electronic states. The shift of the binding energy due to relative surface charging was corrected using the C_{1S} level at 284.8 eV as an internal standard.

2.5. Photocatalytic activity tests

For typical photocatalytic runs, 50 mL of TiO_2 dispersion (1.0 g/L) containing *p*-chlorophenol (4-CP) with concentration of 1.0×10^{-4} M was sonicated for 20 min, and then transferred into a quartz reactor. The percentages of pre-adsorbed substrates in aqueous suspensions of TiO_2 before UV irradiation were below 5% of total amount under equilibrium conditions. The photocatalytic reaction was initiated by a UV LED lamp (CEL-LED100, 365 nm). The intensity of the UV light was measured to be about 9.0 mW cm^{-2}. After turning off the UV illumination, the sample was centrifuged at 10,000 rpm to remove the photocatalyst. The concentration of remaining *p*-chlorophenol was analyzed by a UV spectrophotometer (UV 7504/PC) at the characteristic wavelength (224 nm). No degradation was observed even after 4 h under dark or without photocatalyst.

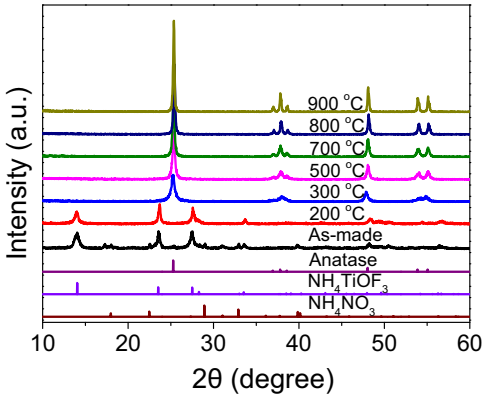

Fig. 1. X-ray diffraction (XRD) patterns of as-made sample and the products upon calcination at different temperature from 200 to 900 °C.

3. Results and discussion

The XRD pattern of as-made microspheres shows strong characteristic diffraction peaks ascribing to NH_4TiOF_3 and weak ones of NH_4NO_3 (Fig. 1), which indicating that the NH_4TiOF_3 is growth during the fast aerosol-spray annealing process. With further a thermal treatment, NH_4TiOF_3 was easily transformed into TiO_2. When the as-made sample is calcined at 200 °C, pure NH_4TiOF_3 phase then appears (Fig. 1). With the annealing temperature increasing, NH_4TiOF_3 phase then completely transforms into anatase TiO_2 at 300 °C (Fig. 1). Further increasing the calcination temperature from 300 to 900 °C, the crystalline phase of anatase remained unchanged except the increased intensity of diffraction peaks of anatase. The formation mechanism of anatase is called topotactic transformation which has been widely reported [8–10,17].

The morphology and crystal structure of the samples were observed by scanning electron microscopy (SEM) and transmission electron microscopy (TEM). The as-made samples calcined at 200 °C (NH_4TiOF_3) shows typical microsphere structure with diameter around a few micrometer (0.5–2 μm) (Fig. 2a) which are composed of plenty of nanosheets (Fig. 2b). The length and width of the nanosheet is about 100–200 and 100–150 nm, respectively, and the thickness is about 10–20 nm. Furthermore, a unique hollow structure is clearly observed (inset of Fig. 2b). After calcination at 500 °C, the morphology and hollow structure keep unchanged reflecting that the sample phase transformed into anatase TiO_2 with no apparent change in morphology. The above phenomenon can be contributed to the similar position of Ti atoms in both crystal structures, and NH_4TiOF_3 could lead to the topotactic transformation to anatase after the removal of N, H, and F atoms from the crystal lattice by a simple heating process [9]. (Fig. 2c and d). A selected-area electron diffraction (SAED) pattern recorded on a nanosheet shows a diffraction pattern of single-crystal anatase along the [001] zone axis (Fig. 2e). Moreover, the porous structure of the TiO_2 nanosheets is confirmed by the TEM image (Fig. 2f). High-resolution TEM (HRTEM) image (Fig. 2g) further shows the single-crystal lattices which clearly demonstrate atomic planes of anatase (200) or (020) crystal faces with the lattice spacing around 0.189 nm [8,9,15–17]. These results suggest that the TiO_2 mesocrys-

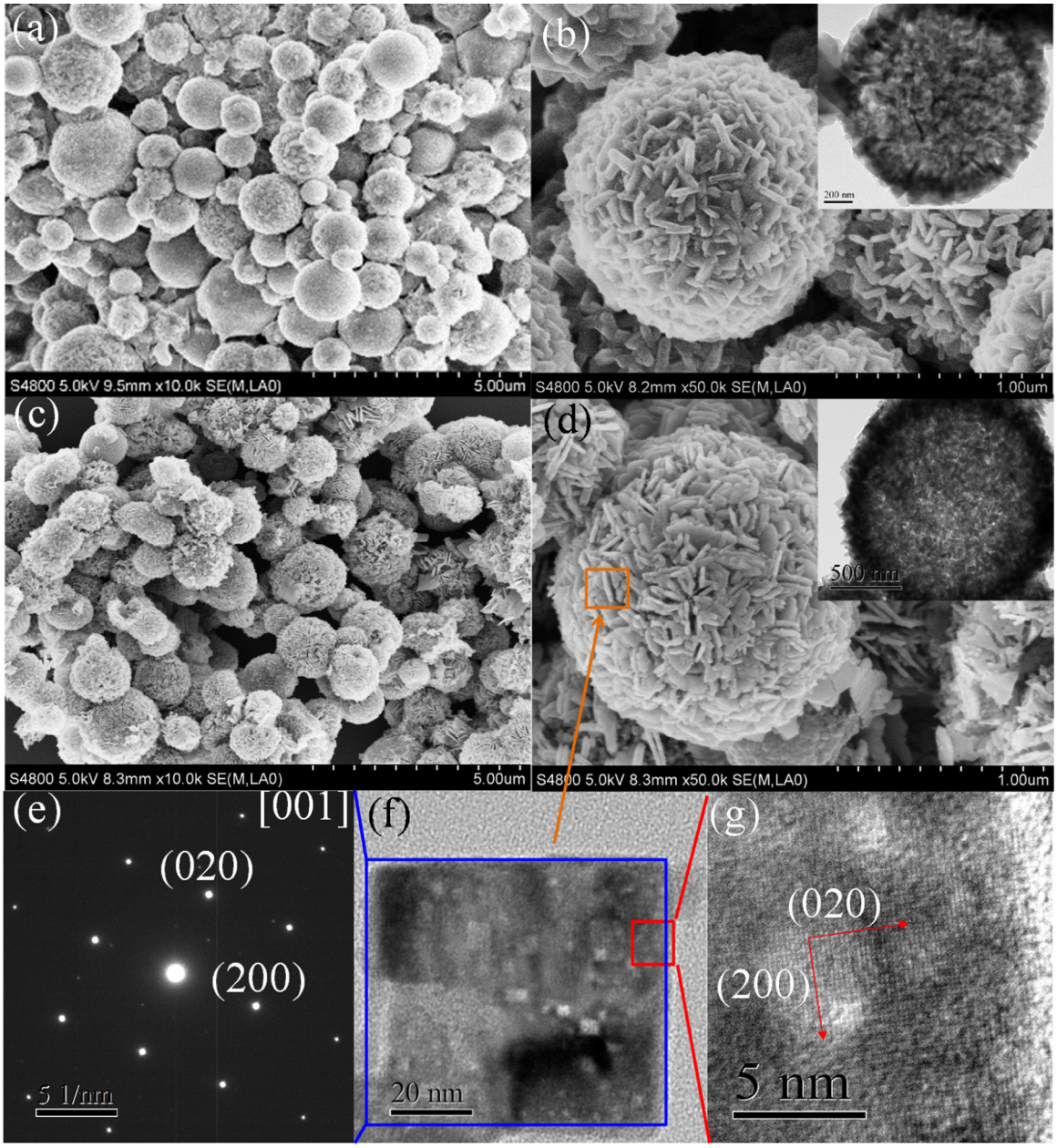

Fig. 2. (a) Scanning electron microscopy (SEM) image and (b) Magnified SEM image of NH_4TiOF_3 hollow microsphere (inset is the TEM image). (c) SEM image and (d) magnified SEM image of the TiO_2 mesocrystal hollow microspheres which were calcined at 500 °C in the air (inset is the TEM image). (e) The selected area electron diffraction (SAED) pattern and (f) TEM image of a representative TiO_2 mesocrystal nanosheet which self-assembled to TiO_2 hollow microspheres. (g) High-resolution TEM (HRTEM) image of the edge of the nanosheet.

tal hollow microspheres are constructed by TiO_2 nanosheets with (001) facet exposure.

Based on the results of SEM images (Fig. 3), the samples retain the hierarchical microsphere morphology with increasing calcination temperatures from 200 – 900 °C. The porosity of as-made sample (NH_4TiOF_3) is very low in terms of the specific surface area (about 2.4 $m^2\ g^{-1}$) and pore volume (0.045 cm^3/g) (Fig. S1 and Table S1). The specific surface area increased to 87 $m^2\ g^{-1}$ after annealing at 300 °C (anatase TiO_2). This reveals the topotactic transformation process from NH_4TiOF_3 into anatase TiO_2 created a large amount of mesopores. However, TiO_2 nanosheets self-assembled into microspheres become thickening and the dimension size shrinks due to the fusion of TiO_2 nanoparticles under the high temperature. The texture properties of TiO_2 mesocrystal miroshperes (Fig. S1 and Table S1) reflect that the specific surface areas and pore volumes gradually decrease from 87 m^2/g, 0.43 cm^3/g to 9.3 m^2/g, 0.022 cm^3/g, respectively. The phenomenon is in good consistence with the crystal size growing of TiO_2 calculated by Scherrer equation (Table S1), indicating the fusion of small TiO_2 crystals into larger ones.

Therefore, the above results promoted us to hypothesize formation mechanism. As illustrated in Fig. S2, the precursor was an aqueous solution containing TiF_4, NH_4NO_3 and P123. The ultrasound-assisted aerosol spray process creates an aerosol mist of liquid droplets. The liquid droplets crystallized into NH_4TiOF_3 nanosheet mesocrystals explosively at a proper temperature (about 250 °C) [9], which also resulted in the concentration gradient within the droplets and thus a hollow microsphere structure formed with evaporating water. Further annealing in the air, NH_4TiOF_3 hollow

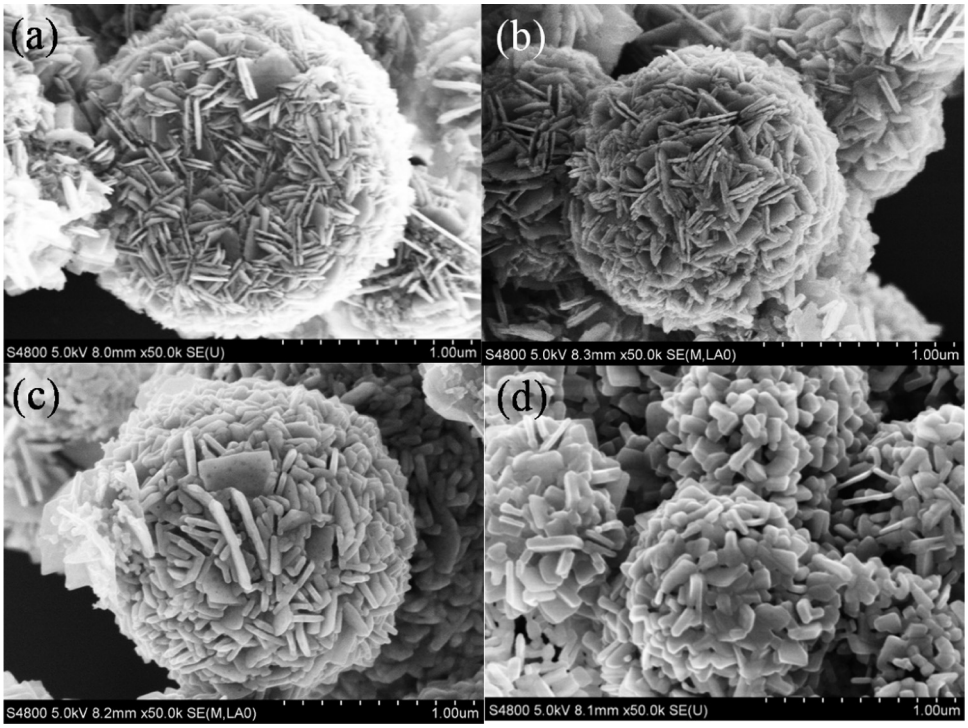

Fig. 3. SEM images of samples annealed at (a) 200 °C, (b) 300 °C, (c) 700 °C, (d) 800 °C.

microspheres were decomposed and topotactic transformed into TiO_2 mesocrystals with the release of gaseous molecules.

Taking into account the principle of aerosol-spray method, the precursors would be transforms into solid materials compulsory without consideration the interactions among different specials in the spherical droplets. Ultrafine Au nanoparticles were easily deposited on hierarchical TiO_2 mesocrystal hollow microspheres by the ultrasonic aerosol-spray method using Au^{3+} precursor solution. It is found that the hierarchical hollow microsphere structure is preserved based on SEM and TEM images (Fig. 4a and b). Moreover, highly dispersed gold nanoparticles were deposited on the surface of TiO_2 as shown in the high-resolution TEM (HRTEM) image (Fig. 4c and d). The size of the gold nanoparticles is about 3–4 nm, while the pore size on each TiO_2 sheet is about 10 nm from the TEM images

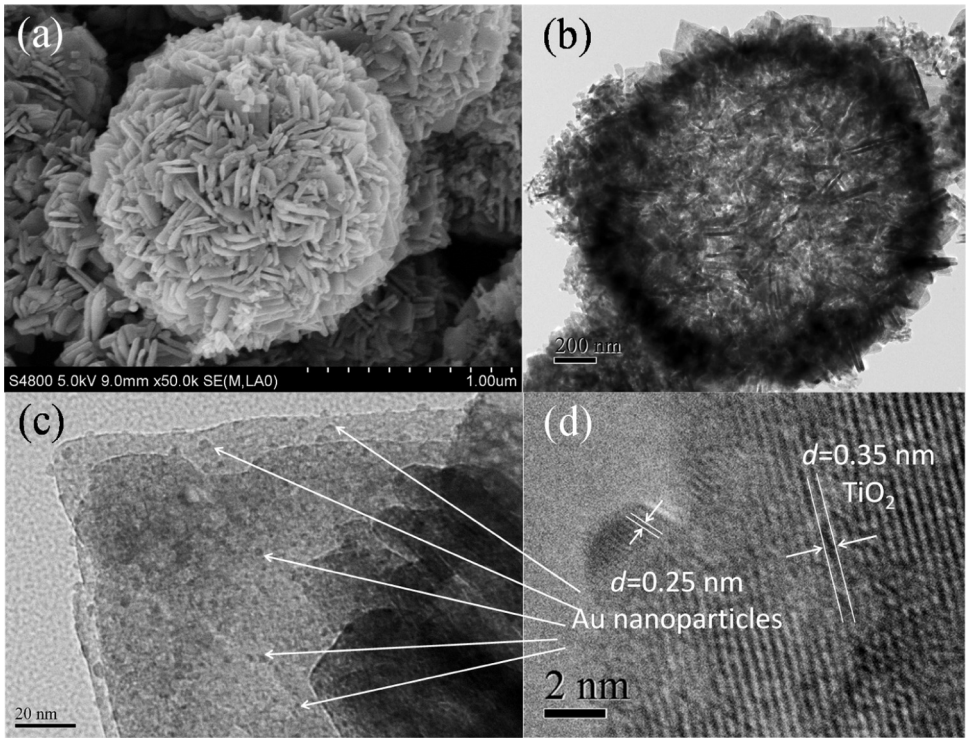

Fig. 4. (a) SEM and (b) TEM images, (c) and (d) High-resolution TEM images of 1.0 *wt* % hollow Au/TiO_2 mesocrystal microspheres.

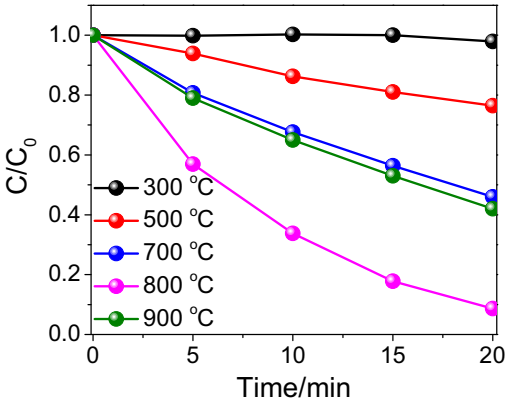

Fig. 5. Liquid-phase photocatalytic degradation of 4-chlorophenol (4-CP) of TiO_2 mesorystal microspheres upon calcination at different temperatures under UV light irradiation.

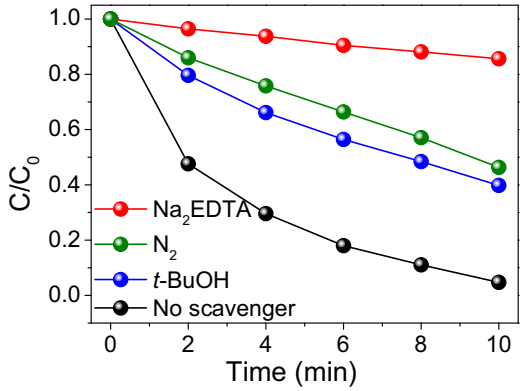

Fig. 7. Photocatalytic degradation of MO with the addition of hole and radical scavenger under UV light irradiation. (1 mM Na_2EDTA and 1 mM *t*-BuOH was added, N_2 bubbling for 20 min).

(Fig. 1f and 1 g) and the pore diameter distribution is about 25 nm which derived from the desorption isotherms. Therefore, the location of Au nanoparticles should be inside of the surface pores of each TiO_2 sheet. After surface deposition by gold nanoparticles, the visible light absorption has greatly improved (Fig. S3).

We used the 4-chlorophenol (4-CP) aqueous solution as the probe to examine the photocatalytic performance of TiO_2 mesocrystals hollow microspheres. The results indicated that the photocatalytic activity of the sample calcined at 800 °C exhibits the highest activity in comparison to these calcined at temperatures in the range of 300–900 °C (Fig. 5 and Fig. S4). Although the specific surface area of TiO_2 mesocrystals decreased drastically, the photocatalytic activity was improved with increasing the calcination temperature from 300 to 800 °C. The impurities (such as N or F) on the TiO_2 surface seriously affect the photocatalytic performance of TiO_2 mesocrystals. X-ray photoelectron spectroscopy (XPS) (Fig. 6) spectra confirmed that the peak around 684 eV and 400 eV belonged to the surface adsorbed F and N species on TiO_2 surface, respectively [9,29–31]. As shown in Fig. 6, the adsorbed F or N species were almost entirely removed after calcination at 600 °C or 800 °C in the air. Owing to the decrease of the specific surface area of the sample calcined at 900 °C, the photocatalytic activity decreased accordingly.

Furthermore, we detected the main oxidative species by using the trapping agents to inhibit active species during the photocatalytic process. As shown in Fig. 7, the addition of *tert*-butanol ashydroxyl radicals (•OH) scavenger, EDTA-Na as holes (h^+) scavenger and N_2 as superoxide anions ($•O_2^-$) scavenger (N_2 will remove dissolved oxygen in solution to inhibit the formation of superoxide anions) were used to investigate photocatalytic degradation performance under UV light irradiation [32,33]. It clearly indicated that the photo-generated holes were the main active oxidative species. EDTA-Na as holes (h^+) scavenger could be greatly prevented the photocatalytic activity which indicated the photocatalytic process was mainly governed by direct holes oxidation reaction. *Tert*-butanol and N_2 as hydroxyl radicals (•OH) and superoxide anions ($•O_2^-$) scavenger also has a certain inhibitory effect on the photocatalytic activity which suggested these radicals were the partial active oxidative species.

Hierarchical TiO_2 mesocrystal hollow microspheres showed superior photocatalytic performance in comparison with nanosheet TiO_2 mesocrystals (Fig. S5a). In the 4-CP oxidation reaction, the photocatalytic efficiency of TiO_2 mesocrystal hollow microspheres shows about 76% higher than that of nanosheet TiO_2 mesocrystals (Fig. 8). This is mainly because the assembled nanosheets are favorable for the multiple-reflection which greatly improves the utilization of UV light [34–39]. If the hollow microsphere structure was destroyed, the crushed sample showed a dramatically decreased activity of 56% which clearly manifests the advantages of the hollow structure (Fig. S5b). In comparison, the photocatalytic performance of TiO_2 mesocrystal hollow microspheres slightly better than the commercial TiO_2 (Degussa P-25) for photocatalytic degradation of 4-CP. The recycling test showed that the TiO_2 mesocrystal hollow microspheres could be used repeatedly for five times without obvious deactivation

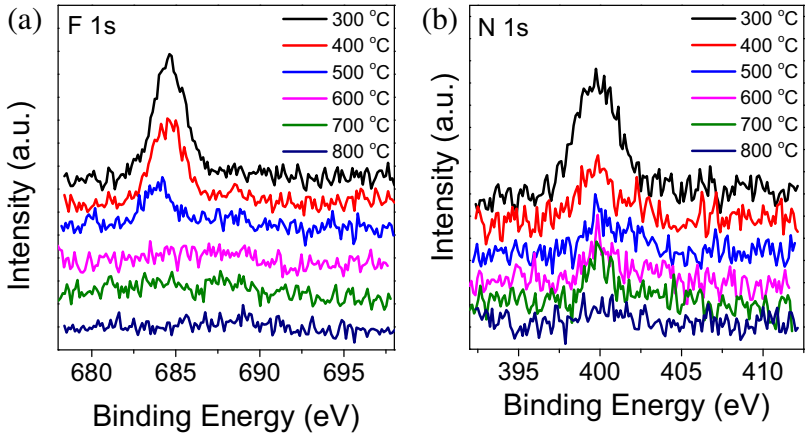

Fig. 6. XPS spectra of TiO_2 mesorystal microspheres calcined at different temperatures.

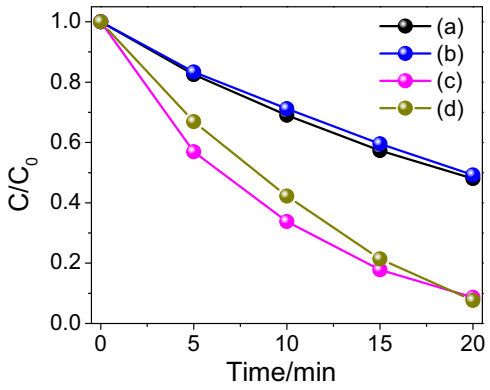

Fig. 8. Liquid-phase photocatalytic degradation of 4-CP on different photocatalysts under UV light irradiation. (a) nanosheet TiO_2 mesorystals, (b) crush sample of hierarchical TiO_2 mesocrystal hollow microspheres calcined at 800 °C, (c) hierarchical TiO_2 mesocrystal hollow microspheres calcined at 800 °C and (d) commercial TiO_2 (P-25).

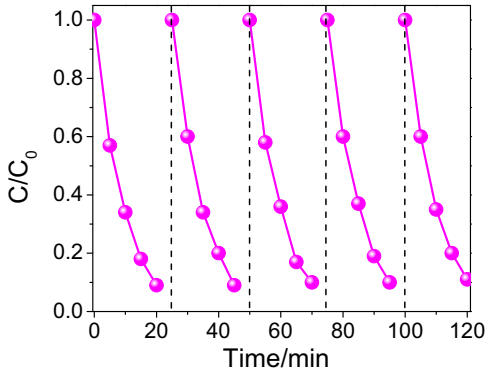

Fig. 9. Recycling tests of hierarchical TiO_2 mesocrystal hollow microspheres calcined at 800 °C under UV light irradiation. (liquid-phase photocatalytic degradation of 4-CP).

(Fig. 9), which showed a high stability of the hollow structure and confirmed by the TEM image (Fig. S6).

4. Conclusions

We have demonstrated an ultrasound-assisted aerosol spray method followed by topotactic transformations upon calcination for preparing hierarchical TiO_2 hollow microspheres which assembled from TiO_2 mesocrystal nanosheets. We found the crystallinity, specific surface area and hollow structure were responsible for the photocatalytic performance of TiO_2 mesocrystal hollow microspheres. Furthermore, ultrafine Au nanoparticle with diameter of 3–4 nm were easily incorporated and well-dispersed on the TiO_2 nanosheets by introducing Au ion precursor at the first step. Au nanoparticle modified TiO_2 mesocrystal hollow microspheres showed greatly enhanced the visible light absorption. The method represents a simple and continued way for the synthesis of TiO_2 mesocrystals which will be great significance for the development and application.

Acknowledgments

This work is supported by National Natural Science Foundation of China (21407106, 21522703), Shanghai Government (14ZR1430800, 13SG44, 15520711300), and International Joint Laboratory on Resource Chemistry (IJLRC). Research is also supported by The Program for Professor of Special Appointment (Eastern Scholar) at Shanghai Institutions of Higher Learning and Shuguang Research Program of Shanghai Education Committee.

Appendix A. Supplementary data

Supplementary data associated with this article can be found, in the online version, at http://dx.doi.org/10.1016/j.apcatb.2016.08.006.

References

[1] X. Chen, S. Shen, L. Guo, S.S. Mao, Semiconductor-based photocatalytic hydrogen generation, Chem. Rev. 110 (2010) 6503–6570.
[2] M.N. Chong, B. Jin, C.W.K. Chow, C. Saint, Recent developments in photocatalytic water treatment technology. A review, Water Res. 44 (2010) 2997–3027.
[3] M.A. Henderson, A surface science perspective on TiO_2 photocatalysis, Surf. Sci. Rep. 66 (2011) 185–297.
[4] S. Linic, P. Christopher, D.B. Ingram, Plasmonic-metal nanostructures for efficient conversion of solar to chemical energy, Nat. Mater. 10 (2011) 911–921.
[5] S. Liu, J. Yu, M. Jaroniec, Anatase TiO_2 with dominant high-energy {001} facets: synthesis, properties, and applications, Chem. Mater. 23 (2011) 4085–4093.
[6] K. Nakata, A. Fujishima, TiO_2 photocatalysis: design and applications, J. Photochem. Photobiol. C 13 (2012) 169–189.
[7] M. Pelaez, N.T. Nolan, S.C. Pillai, M.K. Seery, P. Falaras, A.G. Kontos, P.S.M. Dunlop, J.W.J. Hamilton, J.A. Byrne, K. O'Shea, M.H. Entezari, D.D. Dionysiou, A review on the visible light active titanium dioxide photocatalysts for environmental applications, Appl. Catal. B 125 (2012) 331–349.
[8] Z. Bian, T. Tachikawa, W. Kim, W. Choi, T. Majima, Superior electron transport and photocatalytic abilities of metal-nanoparticle-loaded TiO_2 superstructures, J. Phys. Chem. C 116 (2012) 25444–25453.
[9] Z. Bian, T. Tachikawa, T. Majima, Superstructure of TiO_2 crystalline nanoparticles yields effective conduction pathways for photogenerated charges, J. Phys. Chem. Lett. 3 (2012) 1422–1427.
[10] Z. Bian, T. Tachikawa, P. Zhang, M. Fujitsuka, T. Majima, Au/TiO_2 superstructure-based plasmonic photocatalysts exhibiting efficient charge separation and unprecedented activity, J. Am. Chem. Soc. 136 (2014) 458–465.
[11] F. Chen, F. Cao, H. Li, Z. Bian, Exploring the important role of nanocrystals orientation in TiO_2 superstructure on photocatalytic performances, Langmuir 31 (2015) 3494–3499.
[12] J. Feng, M. Yin, Z. Wang, S. Yan, L. Wan, Z. Li, Z. Zou, Facile synthesis of anatase TiO_2 mesocrystal sheets with dominant {001} facets based on topochemical conversion, CrystEngComm 12 (2010) 3425–3429.
[13] Z. Hong, M. Wei, T. Lan, L. Jiang, G. Cao, Additive-free synthesis of unique TiO_2 mesocrystals with enhanced lithium-ion intercalation properties, Energy Environ. Sci. 5 (2012) 5408–5413.
[14] W. Jiao, L. Wang, G. Liu, G.Q. Lu, H.-M. Cheng, Hollow anatase TiO_2 single crystals and mesocrystals with dominant {101} facets for improved photocatalysis activity and tuned reaction preference, ACS Catal. 2 (2012) 1854–1859.
[15] P. Tartaj, Sub-100 nm TiO_2 mesocrystalline assemblies with mesopores: preparation, characterization, enzyme immobilization and photocatalytic properties, Chem. Commun. 47 (2011) 256–258.
[16] J.-F. Ye, W. Liu, J.-G. Cai, S. Chen, X.-W. Zhao, H.-H. Zhou, L.-M. Qi, Nanoporous anatase TiO_2 mesocrystals: additive-free synthesis, remarkable crystalline-phase stability, and improved lithium insertion behavior, J. Am. Chem. Soc. 133 (2011) 933–940.
[17] L. Zhou, D. Smyth-Boyle, P. O'Brien, A facile synthesis of uniform NH_4TiOF_3 mesocrystals and their conversion to TiO_2 mesocrystals, J. Am. Chem. Soc. 130 (2008) 1309–1320.
[18] Z. Bian, J. Zhu, J. Wen, F. Cao, Y. Huo, X. Qian, Y. Cao, M. Shen, H. Li, Y. Lu, Single-crystal-like titania mesocages, Angew. Chem. Int. Ed. 50 (2011) 1105–1108.
[19] K. Okuyama, I.W. Lenggoro, Preparation of nanoparticles via spray route, Chem. Eng. Sci. 58 (2003) 537–547.
[20] N. Tsapis, D. Bennett, B. Jackson, D.A. Weitz, D.A. Edwards, Trojan particles: large porous carriers of nanoparticles for drug delivery, Proc. Natl. Acad. Sci. 99 (2002) 12001–12005.
[21] D. Arcos, A. Lopez-Noriega, E. Ruiz-Hernandez, O. Terasaki, M. Vallet-Regi, Ordered mesoporous microspheres for bone grafting and drug delivery, Chem. Mater. 21 (2009) 1000–1009.
[22] X. Ji, Q. Hu, J.E. Hampsey, X. Qiu, L. Gao, J. He, Y. Lu, Synthesis and characterization of functionalized mesoporous silica by aerosol-assisted self-assembly, Chem. Mater. 18 (2006) 2265–2274.
[23] X. Jiang, C.J. Brinker, Aerosol-assisted self-assembly of single-crystal core/nanoporous shell particles as model controlled release capsules, J. Am. Chem. Soc. 128 (2006) 4512–4513.

[24] Y. Lu, H. Fan, A. Stump, T.L. Ward, T. Rieker, C.J. Brinker, Aerosol-assisted self-assembly of mesostructured spherical nanoparticles, Nature 398 (1999) 223–226.
[25] Z. Bian, Y. Huo, Y. Zhang, J. Zhu, Y. Lu, H. Li, Aerosol-spray assisted assembly of Bi2Ti2O7 crystals in uniform porous microspheres with enhanced photocatalytic activity, Appl. Catal. B 91 (2009) 247–253.
[26] F. Zhang, C. Kang, Y. Wei, H. Li, Aerosol-spraying synthesis of periodic mesoporous organometalsilica spheres with chamber cavities as active and reusable catalysts in aqueous organic reactions, Adv. Funct. Mater. 21 (2011) 3189–3197.
[27] Y. Yan, F. Zhang, Y. Meng, B. Tu, D. Zhao, One-step synthesis of ordered mesoporous carbonaceous spheres by an aerosol-assisted self-assembly, Chem. Commun. (2007) 2867–2869.
[28] F. Amano, O.-O. Prieto-Mahaney, Y. Terada, T. Yasumoto, T. Shibayama, B. Ohtani, Decahedral single-crystalline particles of anatase titanium(IV) oxide with high photocatalytic activity, Chem. Mater. 21 (2009) 2601–2603.
[29] D. Li, H. Haneda, S. Hishita, N. Ohashi, Visible-light-driven N-F-codoped TiO_2 photocatalysts. 1. Synthesis by spray pyrolysis and surface characterization, Chem. Mater. 17 (2005) 2588–2595.
[30] D. Li, H. Haneda, S. Hishita, N. Ohashi, Visible-light-driven N-F-codoped TiO_2 photocatalysts. 2. Optical characterization photocatalysis, and potential application to air purification, Chem. Mater. 17 (2005) 2596–2602.
[31] Y. Huo, J. Yi, J. Zhu, H. Li, Highly active $TiO_{2-x-y}N_xF_y$ visible photocatalyst prepared under supercritical conditions in NH_4F/EtOH fluid, Appl. Catal. B 89 (2009) 543–550.
[32] F. Zhou, Y. Zhu, Significant photocatalytic enhancement in methylene blue degradation of Bi_2WO_6 photocatalysts via graphene hybridization, J. Adv. Ceram. 1 (2012) 72–78.
[33] B. Jiang, P. Zhang, Y. Zhang, L. Wu, H. Li, D. Zhang, G. Li, Self-assembled 3D architectures of $Bi_2TiO_4F_2$ as a new durable visible-light photocatalyst, Nanoscale 4 (2012) 455–460.
[34] Z. Bian, J. Ren, J. Zhu, S. Wang, Y. Lu, H. Li, Self-assembly of $Bi_xTi_{1-x}O_2$ visible photocatalyst with core-shell structure and enhanced activity, Appl. Catal. B 89 (2009) 577–582.
[35] H. Li, Z. Bian, J. Zhu, D. Zhang, G. Li, Y. Huo, H. Li, Y. Lu, Mesoporous titania spheres with tunable chamber structure and enhanced photocatalytic activity, J. Am. Chem. Soc. 129 (2007) 8406–8407.
[36] K. Li, Y. He, Y. Xu, Y. Wang, J. Jia, Degradation of rhodamine B using an unconventional graded photoelectrode with wedge structure, Environ. Sci. Technol. 45 (2011) 7401–7407.
[37] K. Li, H. Zhang, Y. Tang, D. Ying, Y. Xu, Y. Wang, J. Jia, Photocatalytic degradation and electricity generation in a rotating disk photoelectrochemical cell over hierarchical structured BiOBr film, Appl. Catal. B 164 (2015) 82–91.
[38] G. Liao, S. Chen, X. Quan, Y. Zhang, H. Zhao, Remarkable improvement of visible light photocatalysis with PANI modified core-shell mesoporous TiO_2 microspheres, Appl. Catal. B 102 (2011) 126–131.
[39] J. Zhu, S. Wang, J. Wang, D. Zhang, H. Li, Highly active and durable Bi_2O_3/TiO_2 visible photocatalyst in flower-like spheres with surface-enriched Bi_2O_3 quantum dots, Appl. Catal. B 102 (2011) 120–125.